Hindawi
Journal of Chemistry
Volume 2023, Article ID 8528201, 9 pages
https://doi.org/10.1155/2023/8528201

*Research Article*

# Simulation Study of the Air Separation Performance of Cr-MIL-101 in High-Altitude Environments

**Ying-Chao Wang, Yuan-Zhe Li, Ming-Ming Zhai, Cheng-Cheng Zhao, Kang-Ning Xie, Er-Ping Luo, Chi Tang, and Chen-Xu Zhang**

*Department of Medical Equipment and Metrology, School of Biomedical Engineering, Air Force Medical University, Xi'an 710032, China*

Correspondence should be addressed to Chi Tang; tangchi@fmmu.edu.cn and Chen-Xu Zhang; zhangcx8008@163.com

Received 19 May 2023; Revised 7 September 2023; Accepted 21 September 2023; Published 9 October 2023

Academic Editor: Zhaoqiang Zhang



The most severe challenge for troops in a high-altitude environment is hypoxia. Pressure swing adsorption coupled with membrane separation is an ideal solution for oxygen production in high-altitude areas, but the molecular sieve membranes and organic membranes used in this technique are greatly affected by the ambient temperature, humidity, and pressure. Compared with traditional porous materials, metal-organic frameworks (MOFs) have outstanding features such as low densities, large specific surface areas, high crystallinities, and flexible structures. Cr-MIL-101 (MIL: Matérial Institut Lavoisier) and its derivatives are MOFs with high nitrogen adsorption capacities and can be used for oxygen production by air separation. However, since the plateau climate is complex, the applicability of Cr-MIL-101 for oxygen production in high-altitude environments awaits clarification. Therefore, this study constructed a molecular model of Cr-MIL-101, simulated the adsorption equilibrium of $N_2$ and $O_2$ molecules on this material using the grand canonical Monte Carlo (GCMC) method, and obtained their adsorption isotherms and densities. At 298 K and 100 kPa, the maximum adsorption capacities of Cr-MIL-101 for $N_2$ and $O_2$ were 0.94 per cell and 0.23 per cell, respectively. While at 238 K and 100 kPa, the maximum adsorption amounts of Cr-MIL-101 for $N_2$ and $O_2$ were 5.10 and 1.07 per cell, respectively. The thermodynamic parameters and adsorption equilibrium parameters during the adsorption process were analyzed. The conclusion of this study provides theoretical support for optimizing the $N_2/O_2$ separation performance of Cr-MIL-101 in high-altitude environments.

## 1. Introduction

Oxygen is crucial for maintaining human life activities. After oxygen enters the human body, it combines with hemoglobin in the blood to form oxyhemoglobin and then circulates with the blood to various tissues and organs to generate energy for the normal operation of the tissues and organs [1]. As altitude increases, the partial pressure of oxygen in the atmosphere decreases apparently. When altitudes are higher than 2,700 meters, the human cardiovascular and central nervous systems are affected by hypoxia. Above 4,500 meters, the brain function deteriorates rapidly until loss of consciousness occurs completely.

Xizang Plateau covers an area of 2.5 million square kilometers, accounting for 26.9% of the total land area of China [2]. Most of the Xizang Plateau has elevations of more than 2,700 meters above the sea level, which easily causes altitude sickness. People living in low-altitude areas usually develop symptoms of altitude sickness, such as dyspnea. For hastily arrival at high-altitude areas, the incidence rate is approximately ranging from 25% to 85% [3]. At present, the main treatment methods for acute altitude sickness are oxygen inhalation and hyperbaric oxygen therapy.

There are two main methods for oxygen production in high-altitude areas as follows: cryogenic distillation and pressure swing adsorption combined with membrane separation. Cryogenic distillation techniques and processes are

mature and can produce high-purity oxygen. Therefore, it is currently the most widely used oxygen production method in plain areas. However, this method is not suitable for plateau due to the high energy consumption in oxygen production and the challenges in transporting compressed oxygen cylinders [4]. Pressure swing adsorption combined with membrane separation is an ideal method for oxygen production at plateau due to its advantages, including short construction period for oxygen production equipment, low energy consumption, high degree of automation, and convenient equipment maintenance [5]. This method should be promoted at plateau in the future.

The adsorption and separation performance of molecular sieve and organic membranes under high-altitude conditions is greatly affected by environmental factors such as temperature, humidity, and air pressure. The characteristics of membranes seriously affect the oxygen production efficiency. Therefore, it is necessary to develop a new type of air separation material with high adsorption capacity, good environmental adaptability, and simple preparation process. In the past two decades, metal-organic frameworks (MOFs) have been successfully developed for air separation and received great attention [6]. They are still developing rapidly.

MOFs are new types of organic-inorganic hybrid materials with highly ordered structures. They have enormous development potential and attractive development prospects in gas storage, detection, adsorption- separation, catalysis, drug delivery, sensing, etc., especially in oxygen production through air separation [5], due to their advantages of low densities, large specific surface, high crystallinities, flexible structures, and adjustable pores [7].

MIL-101 (MIL: Matérial Institut Lavoisier), an MOF material containing unsaturated Cr, outperforms Li low-silica X-type (Li-LSX) molecular sieves in $O_2$ and $N_2$ separation. Also, it has an excellent $N_2$ adsorption capacity. Hence, it is applicable for $O_2$ production through air separation [8]. Since high-altitude conditions are harsh with a complex and changeable climate, the applicability of Cr-MIL-101 for $O_2$ production in high-altitude environments must be studied. Therefore, this study will simulate the air separation ability of this material under high-altitude conditions, aiming to provide a reliable theoretical basis for the practical application and optimization of MOFs for $O_2$ production in high-altitude areas.

## 2. Experiment

*2.1. Cr-MIL-101 Model Construction.* The original structure of Cr-MIL-101 was downloaded from the Cambridge Crystallographic Data Centre (CCDC) database. The Cr-MIL-101 topological structure is shown in Figure 1. Cr-MIL-101 consists of two cage structures.One is a regular pentagon, and another is a football structure with alternating pentagons and regular hexagons, where these two types of cages correspond to two different sizes of windows. The regular pentagons are 12 Å, while the regular hexagons are 14.7 Å. The corresponding pore sizes are 29 Å and 34 Å, with a ratio of 2 : 1. The model was imported into Materials Studio

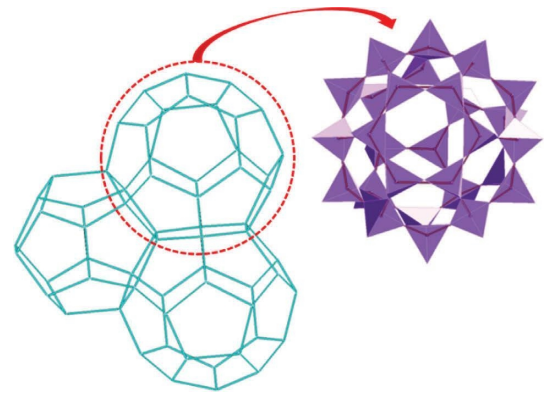

Figure 1: Topological structure of Cr-MIL-101.

to construct the unit cell, as shown in Figure 2(a). To decrease the consumption resources, the unit cell was simplified to a primitive cell.

The structural optimization calculation was performed using the Forcite module of Materials Studio with the Universal force field. Generally, in such calculations, a force field is used to describe the interactions between the adsorbent and adsorbate molecules and the interactions between the adsorbate molecules. The quality of the force field greatly affects the accuracy of the simulation results. Universal force field contains interaction parameters for all elements in the periodic table and can be used to calculate interactions such as adsorption and separation of large systems. The model after structural optimization is shown in Figure 2(b).

*2.2. Adsorbate-Adsorbent Interaction Potential.* In this study, $N_2$ and $O_2$ three-point charge models of the adsorbate molecules were established. To maintain electrical neutrality, the center of each molecule is a virtual atom with only charge and no mass. The models of $N_2$ and $O_2$ molecules (adsorbate molecules) are shown in Figures 3(a) and 3(b). The charge on each N atom in the $N_2$ molecule model is −0.509, and the charge on the virtual atom in the $N_2$ molecule model is +1.018. Also, the charge on each O atom in the $O_2$ molecule model is −0.112, and the charge on the virtual atom in the $O_2$ molecule model is +0.224 [9].

The Lennard–Jones potential function was used in the adsorption simulation process. Assuming that the framework of Cr-MIL-101 and the molecular conformation of the adsorbate remain unchanged during adsorption, only the interactions between frameworks and adsorbate molecules should be considered in the whole system. The interactions include van der Waals and electrostatic. Table 1 lists the parameter settings of the Lennard–Jones potential function and the atomic charges in the framework of Cr-MIL-101 and in the adsorbate molecules [10–12].

## 3. Simulation Method

The Cr-MIL-101 model based on the minimum unit cell was used to simulate the energy and structure of the system. Electrostatic interactions were processed using the Ewald

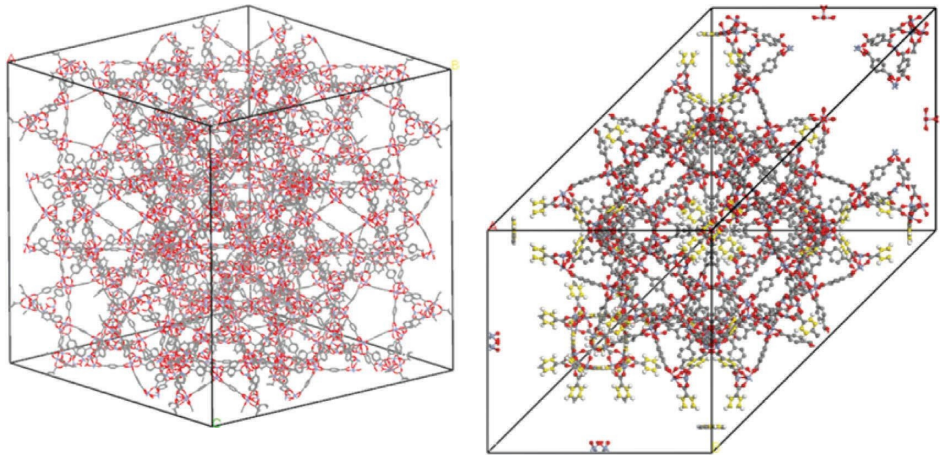

(a) (b)

Figure 2: (a) Unit cell of Cr-MIL-101 constructed using Materials Studio. (b) Cr-MIL-101 model after structural optimization.

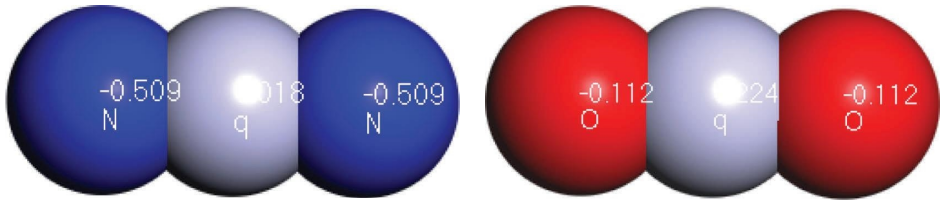


(a) (b)

Figure 3: (a) $N_2$ molecule model and (b) $O_2$ molecule model.

Table 1: Parameter settings of the Lennard–Jones potential function and atomic charges.

| Molecule | Site | $\varepsilon$ (kcal/mol) | $\sigma$ (Å) | Charge |
|---|---|---|---|---|
| $N_2$ | N | 0.072 | 3.724 | −0.509 |
| $O_2$ | O | 0.068 | 3.624 | −0.112 |
| MOF | C_2 | 0.0951 | 3.898 | −0.0481 |
| | C_21 | 0.1467 | 3.983 | −0.0481 |
| | H | 0.044 | 2.886 | +0.37383 |
| | O | 0.0957 | 3.4046 | −0.705 |
| MOF cations | Cr | 0.015 | 3.023 | +3.000 |

summation method with a set precision of $10^{-5}$ kcal/mol. The van der Waals forces were calculated using the atom-based summation method with a cutoff radius of 18.5 Å. In the grand canonical Monte Carlo (GCMC) simulations, the initial configuration was obtained using Metropolis rules. The adsorption isotherm of $N_2$ and $O_2$ on Cr-MIL-101 under conditions of temperatures from 238 to 298 K and pressures from 20 to 100 kPa were obtained for the subsequent derivation and analysis of thermodynamic properties. All simulations in this work were conducted using the Sorption and Forcite modules in Materials Studio.

## 4. Results and Discussion

*4.1. Model Validation.* Based on the model we constructed, the adsorption isotherms of $N_2$ and $O_2$ at 298 K were obtained and compared with experimental results from the literature [8]. The results are shown in Figure 4. The black curves represent simulation results, and red curves represent experimental results. The results shows that the numerical values and trends of the $N_2$ and $O_2$ molecules adsorbed on Cr-MIL-101 are close to the literature data, which demonstrate the accuracy of the model and force field parameters. The method can be used to simulate adsorption at a wider range of temperatures and pressures and to obtain thermodynamic properties such as adsorption isotherms and isosteric heat.

*4.2. Adsorption Isotherm and Adsorption Density.* To simulate the conditions of low temperature and low pressure in high-altitude areas, the temperature range was set to 238 K–298 K and the pressure range was set to 20 kPa–100 kPa, corresponding altitude range from

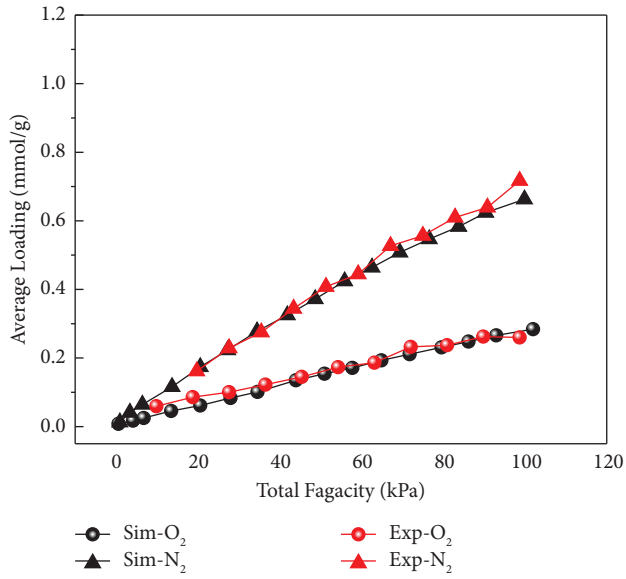


Figure 4: Comparison of simulated $N_2$ and $O_2$ adsorption isotherms and experimental results.

12,000 m to 0 m. The adsorption isotherms of $N_2$ and $O_2$ are shown in Figures 5(a) and 5(b).

According to Figure 5, the adsorption loadings of $N_2$ and $O_2$ on Cr-MIL-101 increase with temperature decreasing, opposite of pressure increasing, which are consistent with the basic adsorption theory. In addition, the adsorption capacity of Cr-MIL-101 for $N_2$ is obviously greater than that for $O_2$, which indicates that Cr-MIL-101 had higher $N_2$ adsorption capacity and lower $O_2$ adsorption capacity. That is beneficial for equilibrium selectivity-based $N_2$ and $O_2$ separation.

Figure 6 shows the adsorption densities of $N_2$ and $O_2$, respectively, at 238 K and 100 kPa. The maximum adsorption capacities of Cr-MIL-101 for $N_2$ and $O_2$ are 5.10 and 1.07 per cell.

Figure 7 shows the adsorption densities of $N_2$ and $O_2$, respectively, at 298 K and 100 kPa. The maximum adsorption amounts of Cr-MIL-101 for $N_2$ and $O_2$ are 0.94 per cell and 0.23 per cell. The adsorption capacities for $N_2$ at 238 K is 5.42 times that at 298 K, and the adsorption capacity of Cr-MIL-101 for $O_2$ at 238 K is 4.64 times that at 298 K. Therefore, the effect of the temperature difference in high-altitude environments on adsorption cannot be ignored.

*4.3. Adsorption Equilibrium Parameters.* Designing and developing porous materials with selective adsorption properties requires an understanding of the adsorption behavior of single components and mixtures. Although single-component adsorption isotherms are convenient to obtain, the accurate measurements of mixture adsorption isotherms are time consuming and difficult. The ideal adsorption solution theory (IAST), proposed by Myers and Prausnitz in 1965, is a method for deriving multicomponent adsorption isotherms from single-component adsorption isotherms [13, 14].

For IAST calculations, pure-component adsorption isotherm data for both gases are necessary. To obtain accurate results in subsequent calculations, the measurement of adsorption isotherm data should be as accurate as possible. Various adsorption models can be used to fit the obtained pure-component adsorption isotherm data to make it functional.

The adsorption equilibrium parameters, which characterize the equilibrium state between the bulk phase and the adsorbed phase, play an important role in the adsorption thermodynamic properties during the separation process. By fitting the adsorption isotherms in Figure 5 with the Langmuir adsorption isotherm equation, which is a model commonly used to explain adsorption isotherms [15], we deduced the adsorption equilibrium parameters.

The Langmuir adsorption isotherm equation is as follows:

$$q_e = q_L \times \frac{K_L \times \mathrm{Ce}}{1 + K_L \times \mathrm{Ce}}, \tag{1}$$

where $q_e$ is the adsorption capacity, $q_L$ is the theoretical single-component saturated adsorption capacity, mg g$^{-1}$; $K_L$ is the Langmuir constant, L mg$^{-1}$, and $q_L$ and $K_L$ reflect the relative affinity of the adsorbate for the adsorbent surface. The Langmuir equation was used to perform regression analysis on the adsorption isotherm data for $N_2$ and $O_2$ on Cr-MIL-101 from 238 to 298 K. The results are shown in Table 2.

S is the selectivity coefficient of the single-component gas $N_2/O_2$, which has the following expression at different temperatures [16]:

$$S = \frac{q_{L1} \times K_{L1}}{q_{L2} \times K_{L2}}. \tag{2}$$

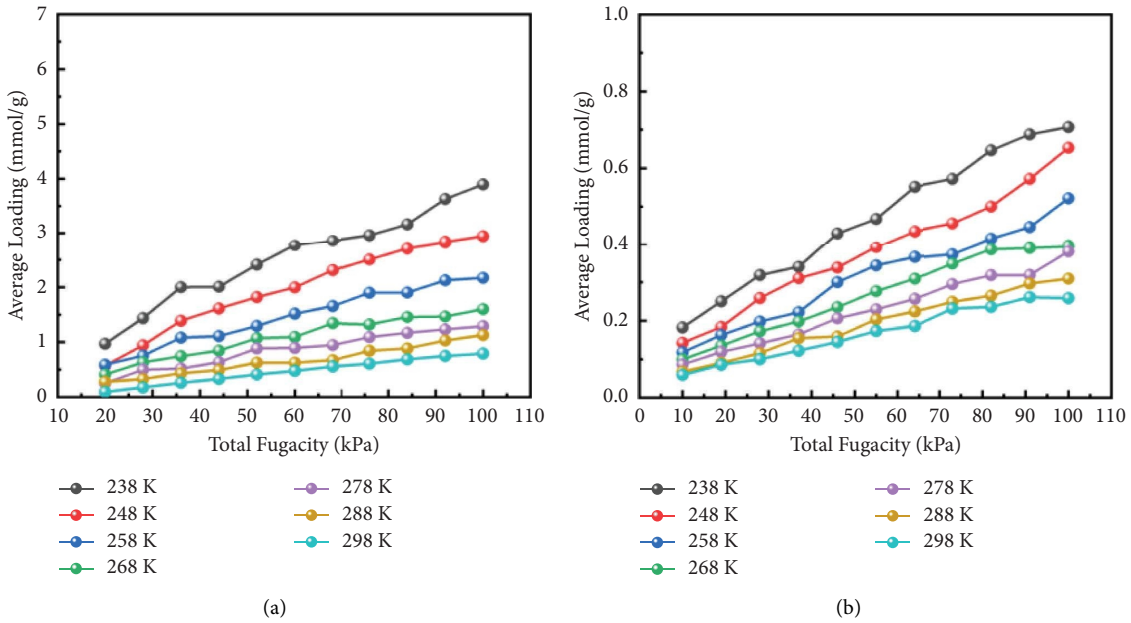


Figure 5: Adsorption isotherms of (a) $N_2$ and (b) $O_2$ at 238–298 K.

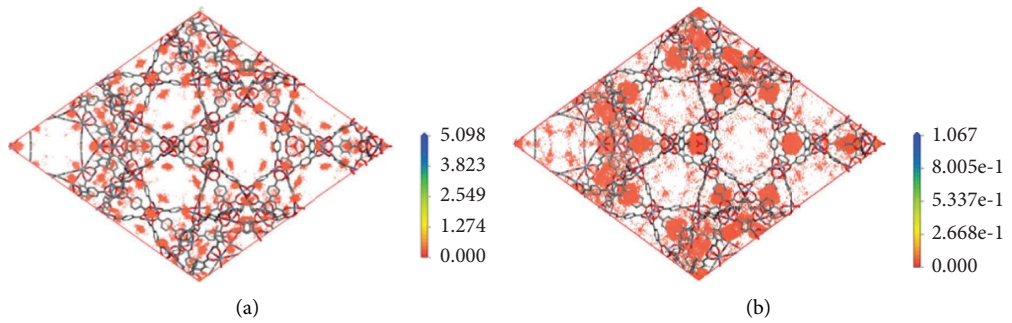


Figure 6: Adsorption density of (a) $N_2$ and (b) $O_2$ at 238 K and 100 kPa.

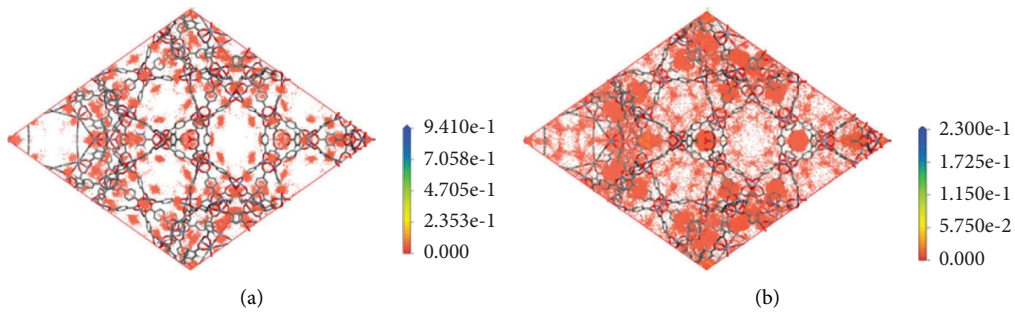


Figure 7: Adsorption density of (a) $N_2$ and (b) $O_2$ at 298 K and 100 kPa.

The variation curve of Cr-MIL-101 shows in Figure 8(a) that the selectivity coefficient S value increases gradually with decreasing temperature at 0.1 kPa and 100 kPa. Interestingly, the selectivity coefficient gradient of Cr-MIL-101 is −0.75%, compared to 5 A zeolite (0.11%), and Li-LSX(5.43%) [5]. This indicates that Cr-MIL-101 has more stable relationship with temperature fluctuation. Also, it is suitable for $O_2$ and $N_2$ separation material at high-altitude areas.

Figure 8(b) shows the selectivity coefficient S decline with decreasing pressure from 100 kPa to 0 kPa. Apparently, S decreases in every temperature. Consistent with the trend of

Table 2: Isotherm fitting results of Cr-MIL-101 from 238 to 298 K.

| T (K) | Gas | Langmuir model | | |
|---|---|---|---|---|
| | | $q_L$ | $K_L$ | $R^2$ |
| 298 | $N_2$ | 41.13633 | 0.000125347 | 0.9875475 |
| | $O_2$ | 0.717732 | 0.005958928 | 0.9767753 |
| 288 | $N_2$ | 3.820489 | 0.001788996 | 0.9719318 |
| | $O_2$ | 0.8428591 | 0.005784134 | 0.9857251 |
| 278 | $N_2$ | 4.119924 | 0.002067344 | 0.9964676 |
| | $O_2$ | 0.9222731 | 0.006383623 | 0.9715641 |
| 268 | $N_2$ | 6.492107 | 0.001513454 | 0.9766884 |
| | $O_2$ | 0.879186 | 0.008685264 | 0.9797441 |
| 258 | $N_2$ | 3.863356 | 0.003380611 | 0.9952929 |
| | $O_2$ | 1.066382 | 0.00823606 | 0.967755 |
| 248 | $N_2$ | 4.38552 | 0.003717685 | 0.9951871 |
| | $O_2$ | 1.462952 | 0.00692409 | 0.9643031 |
| 238 | $N_2$ | 3.691746 | 0.00626844 | 0.991314 |
| | $O_2$ | 1.418926 | 0.009785687 | 0.9771911 |

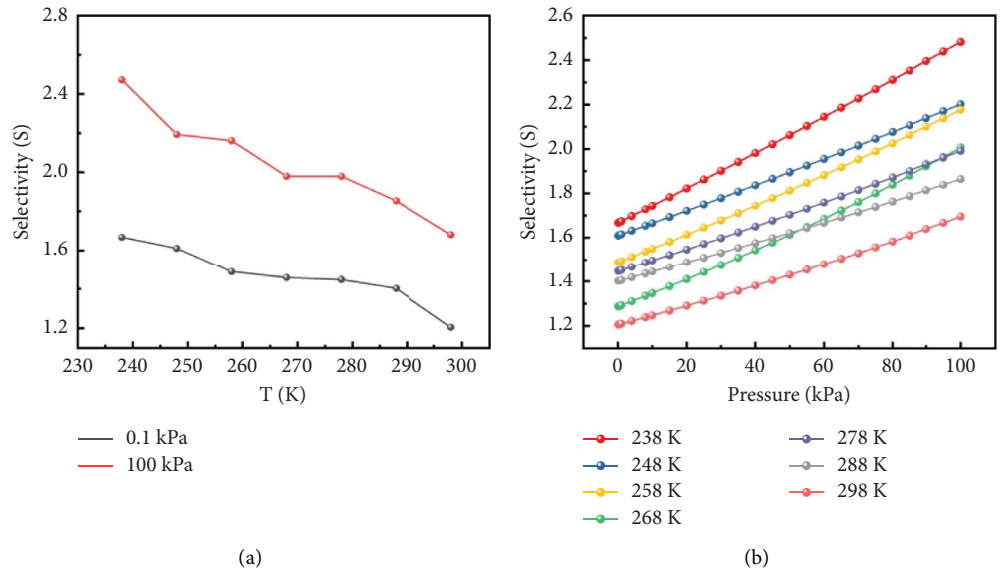


Figure 8: $N_2/O_2$ selectivity of Cr-MIL-101 with (a) increasing temperature and (b) decreasing pressure.

the isotherm, the $N_2/O_2$ selectivity increases with the pressure increased. In addition, the selectivity also increase with the temperature decreased, indicating that the adsorption process is exothermic. The slope of curve is an indicator to illustrate the correlationship between variables. Though linear fitting the curvature, the slope is 0.00479 at 298 K and 0.00810 at 238 K. This means that under room temperature Cr-MIL-101 is steadier than it under low temperature. However, at 248 K, the slope reaches the minimum value of 0.00456. This indicates that the pressure stability first increases and then decreases with temperature rises.

*4.4. Adsorption Thermodynamic Properties.* The isosteric heat of adsorption is a crucial parameter in the adsorption process, and its magnitude reflects the characteristics of the bond-broken and separation process. Since the physical adsorption of gases in porous materials is a spontaneous process, the Gibbs free energy decreases in this process ($\Delta G < 0$). In addition, the entropy is also reduced during this process ($\Delta S < 0$) since the disordered gas molecules are bound on the surface or in the pores of porous materials during this process. According to $\Delta G = \Delta H - T\Delta S$ and $\Delta H = \Delta G + T\Delta S < 0$, the adsorption enthalpy ($\Delta H$) is negative and affected by temperature. Therefore, we can define $\Delta H = -Q_{st}$, where $Q_{st}$ is the desorption enthalpy or isosteric heat of adsorption, which has a positive value [17]. The isosteric heat will change with loading increase because it is greatly affected by the uneven energy distribution on the surface of the adsorbent, and the interactions between adsorbate molecules in the pores cannot be ignored. Therefore, to obtain the $Q_{st}$-$N$ curve, it is necessary to calculate the values of $Q_{st}$ corresponding to different values of adsorption loading ($N$). For each adsorption loading ($N$), its $Q_{st}$ must be calculated [18].

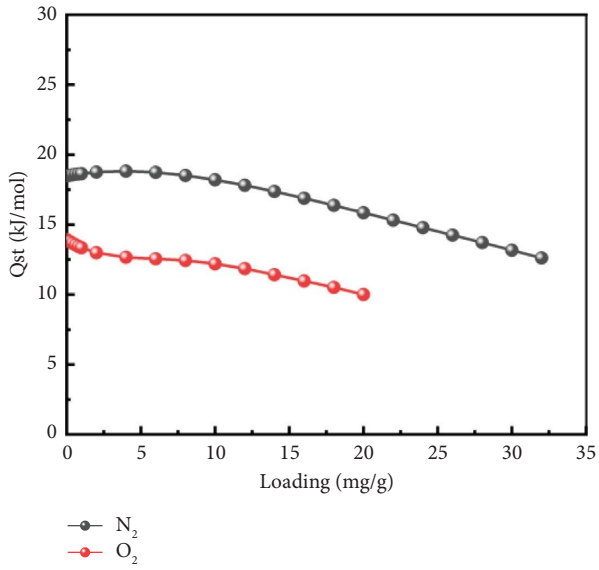


Figure 9: Simulated isosteric heat of $N_2$ and $O_2$ on Cr-MIL-101 at 238 K.

At a certain adsorption capacity, the relationship between pressure $P$ and temperature $T$ can be expressed by the following virial equation [19]:

$$\ln P = \ln N + \frac{1}{T} \times \sum_{i=0}^{m} a_i N^i i + \sum_{j=0}^{n} b_j N^j, \quad (3)$$

where $N$ is the adsorption loading, and $a_i$ and $b_j$ are empirical parameters independent of temperature.

The following expression [20] can be used to calculate the isosteric heat of adsorption ($Q_{st}$):

$$Qst = -R \sum_{i=0}^{m} a_i N^i. \quad (4)$$

When the temperature range is sufficiently small, $Q_{st}$ can be assumed to be independent of temperature. Then, adsorption isotherms measured by two or more sets of experiments can be used to calculate $Q_{st}$. Here, two sets of temperature data, 238 K and 248 K, were used to calculate the isosteric heat of $N_2$ and $O_2$ on Cr-MIL-101 at 238 K.

Figure 9 shows the simulated isosteric heat of $N_2$ and $O_2$ on Cr-MIL-101 at 238 K. Obviously, the adsorption process belongs to physical adsorption. The isosteric heat gradually decreases with increasing adsorption loading, which indicates that low-temperature conditions are more favorable for the adsorption performance of Cr-MIL-101. The decrease rate for $N_2$ and $O_2$ are 18.6% and 16.9%, respectively. That means when temperature and pressure decrease, both the adsorption amounts of $N_2$ and $O_2$ decrease at the same time. But the drop in nitrogen is even greater, which leads to the decline of S, that is, consistent with the IAST results.

Through GCMC simulation calculations, the potential energy distributions of $N_2$ and $O_2$ on Cr-MIL-101 at 238 K and 298 K were obtained, as shown in Figure 10. The difference of quadrupole moment makes $N_2$ and $O_2$ selectively adsorbed on Cr-MIL-101. The electrostatic

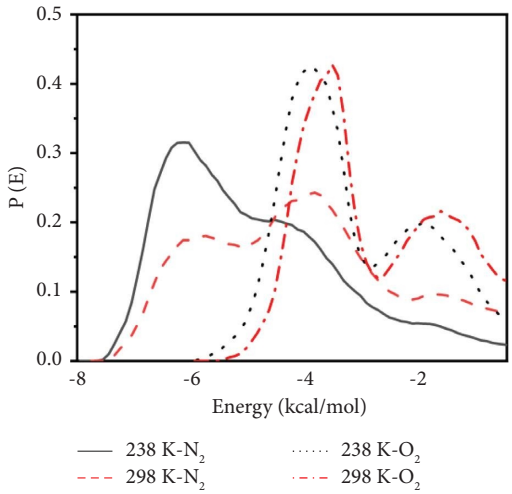


Figure 10: Potential energy distributions of $N_2$ and $O_2$ on Cr-MIL-101 at 238 and 298 K.

interactions between $N_2$ molecules and metal cations are stronger than that of $O_2$. The potential energy distributions of $N_2$ and $O_2$ molecules adsorbed on Cr-MIL-101 are greatly affected by the distribution of adsorption sites in the interior space of the adsorbent. The interaction energy between the adsorbate molecules and adsorbents increases with temperature decreasing, but its distribution does not change with temperature. Figure 10 shows that the adsorption of $N_2$ by Cr-MIL-101 occurs mainly in two concentrated regions, the potential energy distribution of $N_2$ has two peaks, and the $O_2$ molecules are distributed in regions with lower potential energy. Notably, the peak intensities of the potential energy distributions of $N_2$ at 238 K and 298 K differ greatly, which indicates that the adsorption sites of $N_2$ in the pores have a weaker binding capacity for $N_2$ at 298 K than at 238 K.

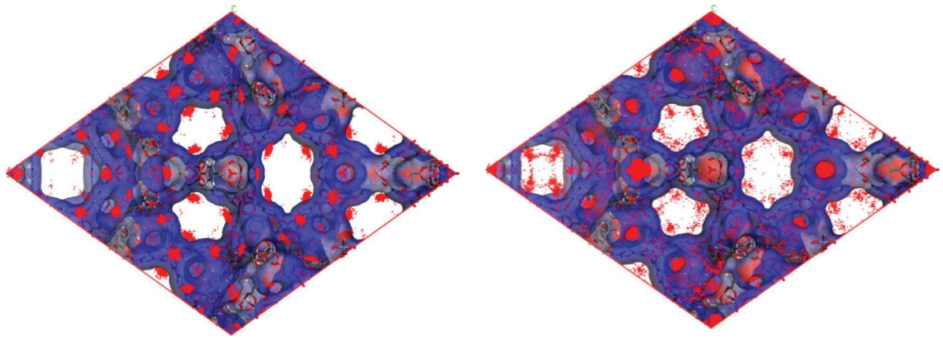

(a) (b)

Figure 11: Adsorption density of (a) $N_2$ and (b) $O_2$ at 238 K and 100 kPa.

As shown in Figure 11, to obtain more intuitive structural information on different adsorption sites in the pores of Cr-MIL-101, the three-dimensional potential energy surfaces of $N_2$ and $O_2$ at 238 K were superimposed on the equal-adsorption density planes. $N_2$ and $O_2$ molecules distributed closer to red areas have higher adsorption interaction energies, and those distributed closer to blue areas have lower adsorption interaction energies. Through this method, the active adsorption sites of $N_2$ and $O_2$ molecules can be identified directly on the map. The color contrast between $N_2$ and $O_2$ is clearly large. On Cr-MIL-101, the absolute value of the potential energy of $N_2$ is higher than that of $O_2$. These results are consistent with the simulated adsorption isotherms.

## 5. Conclusions

In this study, a molecular model of Cr-MIL-101 was constructed, the adsorption equilibrium of $N_2$ and $O_2$ on this material was calculated by the GCMC simulation method, and the adsorption isotherms and adsorption densities were determined. Thermodynamic parameters such as the adsorption potential energy distribution and isosteric heat, as well as adsorption equilibrium parameters such as the adsorption energy and selectivity, were obtained. The findings of this study provide theoretical support for optimizing the $N_2/O_2$ separation performance of Cr-MIL-101 in high-altitude environments.

## Data Availability

The datasets used and/or analyzed to support the findings of this study are available from the corresponding author on reasonable request.

## Disclosure

Ying-chao Wang and Yuan-zhe Li are the co-first authors.

## Conflicts of Interest

The authors declare that there are no conflicts of interest.

## Authors' Contributions

Ying-chao Wang conceptualized the paper. Yuan-zhe Li drafted the manuscript. Chen-xu Zhang supervised the project. Ming-ming Zhai drafted a part of the manuscript. Cheng-cheng Zhao drew a part of the figures. Kang-ning Xie reviewed the manuscript and corrected the grammar error. Chi Tang and Er-ping Luo edited the manuscript finally. Ying-chao Wang and Yuan-zhe Li contributed to the work equally.

## Acknowledgments

This research was funded by Medical Equipment Research Project (KJ2017A05193) and NSF of Shaanxi Province (2023-YBGY-163).

## References

[1] L. Chen, Z. Yang, and H. Liu, "Hemoglobin-based oxygen carriers: where are we now in 2023?" *Medicina*, vol. 59, no. 2, p. 396, 2023.

[2] C. Fang, "How to promote the green development of urbanization in the Tibetan Plateau?" *Journal of Geographical Sciences*, vol. 33, no. 3, pp. 639–654, 2023.

[3] K. M. Poudel, T. R. Poudel, N. Shah et al., "Ascent rate and the Lake Louise scoring system: an analysis of one year of emergency ward entries for high-altitude sickness at the Mustang district hospital, Nepal," *PLoS One*, vol. 17, no. 10, Article ID 0276901, 2022.

[4] K. Gopalsamy and R. Babarao, "Heterometallic metal organic frameworks for air separation: a computational study," *Industrial & Engineering Chemistry Research*, vol. 59, no. 35, pp. 15718–15731, 2020.

[5] Y. Fu, Y. Liu, X. Yang et al., "Thermodynamic analysis of molecular simulations of $N_2$ and $O_2$ adsorption on zeolites under plateau special conditions," *Applied Surface Science*, vol. 480, pp. 868–875, 2019.

[6] F. Yang, Y. Gao, H. Pang et al., "Applications of metal-organic frameworks in water treatment: a review," *Small*, vol. 18, no. 11, Article ID 2105715, 2022.

[7] Y. Peng, J. Xu, J. Xu et al., "Metal-organic framework (MOF) composites as promising materials for energy storage applications," *Advances in Colloid and Interface Science*, vol. 307, Article ID 102732, 2022.

[8] F. Zhang, H. Shang, L. Wang et al., "Substituent-induced electron-transfer strategy for selective adsorption of $N_2$ in MIL-101(Cr)-X metal-organic frameworks," *ACS Applied Materials & Interfaces*, vol. 14, no. 1, pp. 2146–2154, 2022.

[9] A. J. Richards, K. Watanabe, N. Austin, and M. R. Stapleton, "Computer simulation of the gas separation properties of zeolite Li-X," *Journal of Porous Materials*, vol. 2, no. 1, pp. 43–49, 1995.

[10] K. Watanabe, N. Austin, and M. R. Stapleton, "Investigation of the air separation properties of zeolites types A, X and Y by Monte Carlo simulations," *Molecular Simulation*, vol. 15, no. 4, pp. 197–221, 1995.

[11] P. Cosoli, M. Ferrone, S. Pricl, and M. Fermeglia, "Hydrogen sulphide removal from biogas by zeolite adsorption: Part I. GCMC molecular simulations," *Chemical Engineering Journal*, vol. 145, no. 1, pp. 86–92, 2008.

[12] N. A. Ramsahye and R. G. Bell, "Cation mobility and the sorption of chloroform in zeolite NaY: molecular dynamics study," *Journal of Physical Chemistry B*, vol. 109, no. 10, pp. 4738–4747, 2005.

[13] A. L. Myers and J. M. Prausnitz, "Thermodynamics of mixed-gas adsorption," *AIChE Journal*, vol. 11, no. 1, pp. 121–127, 1965.

[14] K. S. Walton and D. S. Sholl, "Predicting multicomponent adsorption: 50 years of the ideal adsorbed solution theory," *AIChE Journal*, vol. 61, no. 9, pp. 2757–2762, 2015.

[15] N. Ayawei, A. N. Ebelegi, and D. Wankasi, "Modelling and interpretation of adsorption isotherms," *Journal of Chemistry*, vol. 2017, Article ID 3039817, 11 pages, 2017.

[16] G. F. Bennett, "Adsorbents: fundamentals and ApplicationsRalph T. Yang, john wiley & sons, hoboken, NJ, 2003, US$dollar; 94.95, 422 pp., ISBN: 0-471-29741-0," *Journal of Hazardous Materials*, vol. 109, no. 1–3, pp. 227-228, 2004.

[17] J. Zhang, C. Wei, C. Zhao, T. Zhang, G. Lu, and M. Zou, "Effects of nano-pore and macromolecule structure of coal samples on energy parameters variation during methane adsorption under different temperature and pressure," *Fuel*, vol. 289, no. 1, Article ID 119804, 2021.

[18] S. P. D. Monte Blanco, F. B. Scheufele, A. N. Módenes et al., "Kinetic, equilibrium and thermodynamic phenomenological modeling of reactive dye adsorption onto polymeric adsorbent," *Chemical Engineering Journal*, vol. 307, pp. 466–475, 2017.

[19] L. Czepirski and J. JagieŁŁo, "Virial-type thermal equation of gas-solid adsorption," *Chemical Engineering Science*, vol. 44, no. 4, pp. 797–801, 1989.

[20] F. R. Siperstein, C. Avendaño, J. J. Ortiz, and A. Gil-Villegas, "Analytic expressions for the isosteric heat of adsorption from adsorption isotherm models and two-dimensional SAFT-VR equation of state," *AIChE Journal*, vol. 67, no. 3, Article ID 17186, 2021.